MANUSCRIPT COVER PAGE FORM

E-MRS Symposium : O

Paper Number : O - 147

Title of Paper : CHARACTERIZATION OF THE CHEMICAL BATH DEPOSITED $In(OH)_xS_y$ FILMS: IMPORTANCE OF THE GROWTH CONDITIONS

Corresponding Author: T. Dedova

Full Mailing Address: Department of Materials Science

Tallinn University of Technology

Ehitajate tee 5, Tallinn 19086

Estonia

Telephone : + 372 6203369

Fax : + 372 6203367

E-mail : dedova@staff.ttu.ee

CHARACTERIZATION OF THE CHEMICAL BATH DEPOSITED $In(OH)_xS_y$ FILMS: IMPORTANCE OF THE GROWTH CONDITIONS

T. Dedova[1,2)], J.Wienke[1)], M. Goris[1)], M. Krunks[2)]

1) *ECN Energy research Centre of the Netherlands, P.O. Box 1, 1755 ZG Petten, The Netherlands*

2) *Department of Materials Science, Tallinn University of Technology, Ehitajate tee 5, Tallinn 19086, Estonia*

Abstract

The $In(OH)_xS_y$ thin films were deposited by chemical bath deposition using three different deposition procedures: 'hot': starting the deposition at 70°C, 'cold': starting the deposition at room temperature and pre-treatment with In^{3+} ions prior the 'hot' deposition. The analysis of the deposited $In(OH)_xS_y$ layers on glass revealed that modifications in the chemical bath deposition procedure provoked significant changes in the nucleation process, the growth rate, the layer elemental composition and the layer morphology. With an additional In^{3+} pre-treatment or starting from a cold solution, the formation of a dense bottom layer has been observed, resulting in a more compact structure and the refractive index values of 2.6, compared to those obtained from 'hot' deposition. The comparison of the measured In/S ratio with a thicker layer suggests, that the $In(OH)_xS_y$ deposition starts with an OH-rich layer. Assuming the indirect allowed bang gap transition type, an Eg of 2.2 eV was found independent of the procedure type, deposition time or films thickness.

Keywords: chemical bath deposition (CBD), $In(OH)_xS_y$, thin film, growth rate, optical bandgap, refractive index

1. **Introduction**

CdS is well-known as most efficient and frequently used buffer layer in a chalcopyrite absorber (CIGS, CIS) based solar cells [1]. However, in order to remove the toxic cadmium the development of alternative buffer layers has become a main issue of nowadays research. It has been shown, that solar cells based on chemical bath deposited In(OH)xSy buffer layer reached a conversion efficiency of 15.7% with a $Cu(In,Ga)Se_2$-absorber [2] and 11.4% efficiency with $CuInS_2$ as absorber [3].

From the CdS deposition is known that the CBD processing has a significant influence on the final buffer layer functioning. Delaying the thiourea decomposition, e.g. by starting the CBD process at room temperature [4] leads to initial cadmium hydroxide formation and subsequent CdS deposition. Moreover the exclusive Cd-ion treatment has extensively been described [5,6] and has also been used as pre-treatment before subsequent buffer layer deposition [7]. Few articles already [8,9] refer to the beneficial effect of an In-ion treatment on the CIGS and CGS surfaces without or with the following buffer layer deposition [10]. Kaufmann [11] has published that $In(OH)_3$ nanocolloids formed in the bath during In(OH)xSy deposition act as a nucleation centres which are apparently of importance to the film growth and properties.

This work is devoted to the study of above-mentioned CBD conditions, such as a delayed sulphur supply or, in this case, an In-pretreatment, on the In(OH)xSy formation.

In our study we define three different In(OH)xSy deposition procedures:

'hot': starting the deposition at 70°C, 'cold': starting the deposition at room temperature and 'In+hot': In-ions pretreatment prior the 'hot' deposition.

In addition to the study of In(OH)xSy growth and morphology the optical properties of the films, as well as the evolvement of the refractive indices have been determined in dependence of the above-mentioned CBD conditions.

2. Experimental

2.1. Chemical bath deposition

$In(OH)_xS_y$ films were applied by chemical bath deposition on bare soda-lime glass microscope slides. The glass was cleaned with isopropyl alcohol during 5 minutes in ultrasonic bath and then boiled in deionized water for 10 minutes.

An aqueous solution of indium chloride ($InCl_3$, 0.025 M/L), thioacetamide (TAA, 0.3 M/L) and acetic acid (0.2 M/L) was used. Our experimental conditions of the reagents concentrations and bath temperature of 70°C are similar to those of Bayon et al. [12] used for $In(OH)_xS_y$ deposition.

The substrates were subsequently taken out after every 10 minutes, the maximum deposition time was 60 minutes. Obtained films were rinsed with double distilled water and dried in an argon flow.

Chemical bath deposition was carried out by three different deposition processes: 'hot' start - starting the deposition at 70°C using pre-heated solutions (further "A"), 'cold' start – starting the deposition at room temperature (B), and In^{3+}-pretreatment prior the subsequent 'hot' deposition (C). Indium pre-treatment of the substrates was carried out during 10 minutes in the indium chloride solution at 70 ºC.

2.2. Films characterization

The surface morphologies of the films were examined by JEOL JSM-6330F Field Emission Scanning Electron Microscope (SEM) (cold-cathode field emission) with a resolution of 2 nm at 5kV. The elemental composition of the films was studied by the X-ray dispersive microanalysis (EDX) using the accelerating voltage 15 kV.

The UV–VIS transmission and reflection spectra have been taken with a spectro 320 R5 apparatus (Instrument Systems GmbH) equipped with integrating sphere in the wavelength

region from 250 to 1400 nm. Obtained data were used to calculate the absorption coefficient (α), optical bandgap (E_g).

The thickness and refractive indices values were obtained using specular reflectance measurements recorded on Filmetrics F20 using Cauchy fitting method. Cross-section micrographs from selected samples were also used to evaluate the films thicknesses. Accuracy of obtained refractive indices was controlled by additional calculation using interference-fringe method [13].

3. Results and discussion

3.1. Morphological study and composition analysis

The following section describes the morphology evolvement of the layers by the three above-defined processes. The SEM photographs show the deposition of some random particles on the surface of glass for the A process (Fig. 1a). For the B-process the same particles have been detected after the underlayer has been formed (Fig. 1b) and in the C process these particles have also been observed on the preformed underlayer after only 5 minutes of deposition (Fig. 1c). EDX analysis of such a partially deposited layer on an underlayer following procedure C results in a S/In atomic ratio of 0.6, indicating negligible incorporation of sulphur in the initial phase. Kaufmann et al. suggested [11] that within the first 10 minutes of deposition the $In(OH)_3$ is more dominant than the oxide or sulphide phase. With prolonged deposition time, the particle density increases and the particles start to coalesce until after ca. 30 minutes a closed layer has been formed. The hot start procedure (Fig. 2a) resulted in a more porous layer having fibrous like morphology film. Some open areas still could be seen even after 30 minutes of deposition. This confirms the observations of Yamaguchi [14], who describes the formation of porous and rough $In(OH)_xS_y$ films with increasing deposition time. The films obtained after 30 minutes in bath C show a compact structure with a thickness 160 nm (Fig. 2c). In comparison to procedure A and C, the cold start procedure (B) delivers also dense layers, as is obvious from Fig. 2b. These films have a special cauliflower like morphology, which is presumably a result of the comparably low layer growth rate. Films with similar morphologies have been found by Yamaguchi for slow depositions at T=30ºC. The S/In molar ratio determined by EDX for a closed layer formed with procedure B is 1.2, indicating a higher sulphur amount, but the final S/In-ratio is still lower than 1.5, as it would be expected

for In_2S_3. This result and the found composition gradient in the layer are both in agreement with other works on the CBD deposition of $In(OH)_xS_y$ layers [11,15, 16, 17].

As it has been shown in inset of Fig. 1c, a so-called 'partial' treatment with solely indium leads already to the formation of a dense approximately 25 nm thick layer. Even more thin dense underlayer was observed for cold start procedure (inset of Fig. 1b) after 10 minutes of deposition. In order to get more information whether $In(OH)_3$ has been deposited, the In-treatment has been carried out on a nanoporous TiO_2 layer with an approximately 100-fold higher surface area. The 10 minutes In-treated substrates were exposed to a 0.5 M thioacetamide solution and after 30 minutes the layers became yellow coloured indicating the conversion eventually formed $In(OH)_3$ into the sulphide phase.

3.2. Thickness determination and films growth rate

The films thicknesses were calculated using specular reflectance spectra and Cauchy fitting model (Fig. 3). Additional to that some cross-section micrographs were taken for comparison and both methods were in good agreement.

As it can be seen from the growth rate curves (Fig. 4), the kinetics of the processes A and C follow a sigmoidal profile, which corresponds to typical kinetics of a CBD process and is characteristic for autocatalytic reactions [18,19]. This process includes three main phases: initiation phase with formation of nuclei, film growth, catalysed by the nucleation centres, and a termination step where the reaction slows down and finally stops. The growth rate for the In-pretreated series (C) is much faster compared to the A and B procedures. Extrapolating the growth rate curve to the ordinate would reveal a starting thickness of 23 nm, which is in agreement with the SEM cross section value found after the initial In-treatment (Fig. 1c). It is known that initial nucleation has significant influence on the film growth rate and properties; the reaction rate increases resulting also in a higher terminal thickness. The shorter induction period for C process, compare to A confirms the catalysing effect of the initial layer. The

termination phase begins for the C process at 45 minutes, if a layer thickness of 225 nm has been reached. For process A the saturation starts at 55 minutes, if a thickness of 170 nm has been reached. The cold start reaction shows approximate linear and slow growth rate over the entire deposition period. This could be explained by a delayed thioacetamide decomposition, which starts only at temperatures higher than 40ºC. Below 40ºC the $In(OH)_3$ hydroxide formation determines the reaction and the mechanism of $In(OH)_xS_y$ formation could be similar to those proposed for CdS film formation [20, 21]. The $In(OH)_3$ nuclei, adsorbed at the substrate surface bound in a later metathetical reaction the deliberated sulphur ions in a heterogeneous process, finally forming $In(OH)_xS_y$.

3.3. Optical properties and band gap energy determination

The Eg values were calculated using well-known equation:

$$\alpha h\nu = A(h\nu - E_g)^{\frac{1}{n}},$$

Where the absorption coefficient α was calculated from the transmittance and reflectance spectra, the band gap Eg has been extracted after extrapolation of the linear region of $(\alpha h\nu)^n$ plot on the hν axis, n is the exponent which depends on the nature of the optical transition type ($n = \frac{1}{2}, \frac{1}{3}, 2, \frac{2}{3}$) for allowed and forbidden indirect and for allowed and forbidden direct transitions, respectively and A is a constant associated with the transition probability.

The optical transition type of $In(OH)_xS_y$ films is a matter of discussions in the literature. Some of the authors reported [22, 23, 24] a high Eg of app. 2.6-2.8 eV, assuming the direct transition type. Another group of authors [11, 24, 25] proposed the indirect transition type and report Eg values of 2.1-2.2 eV. We assume the indirect transition type as the linearity of $(\alpha h\nu)^{1/2}$ vs. hν plot is more evident compared to the $(\alpha h\nu)^2$ vs. hν plot for direct allowed transition types. Following to Bhattacharyya [26] and plotting the log (αhν) vs. log (hν-Eg) a clear linear behaviour with slope of 2 has been found (inset of Fig. 5) , which coincides with indirect allowed transition type.

The Eg values calculated for the deposited $In(OH)_xS_y$ layers are approximately 2.1 – 2.2 eV, independent of the procedure type, deposition time or the films thickness. A possible explanations why we couldn't observe the underlayer existence from optical measurements could be its high bandgap value of 5.15 eV (monocrystalline $In(OH)_3$) [27], which is not possible to detect due to glass absorption edge.

Films deposited up to 25 minutes for B and C processes show a high optical transmittance of 90% in the visible light region, whereas prolonged deposition times resulted in lower transmittance values of 80-75% in the wavelength region of 500 to 1400 nm. Films obtained from A procedure show a comparably lower transmittance of 80% even at shorter deposition times.

We found that the refractive indices are in the range of 2.2 slightly decreasing (±0.1) with increasing deposition times for hot start procedure. The values are higher than those reported by Bayon [28]. Films obtained from a pretreated bath (C) showed refractive indices of 2.6 giving an additional indication for their more compact structure and are in a good agreement with those reported for In_2S_3 thin films [29].

4. Conclusions

We have demonstrated that the CBD conditions for the $In(OH)_xS_y$ deposition are crucial for the final layer formation. In comparison to a standard 60 ºC CBD process, in case of starting a chemical $In(OH)_xS_y$ deposition from a cold bath or if a partial indium pre-treatment is given to the substrate a dense indium hydroxide underlayer has formed. This initial or incubation layer catalyses the growth and effects the final $In(OH)_xS_y$ layer morphology. For the layers obtained from a cold bath or with an In-pretreatment a more compact structure has been observed by SEM analysis and the refractive index values of 2.6 are significantly higher than the value of 2.2 calculated for a film formed by the 'hot' start procedure. Assuming the indirect allowed bang gap transition type, an Eg of 2.2 eV was found independent of the

procedure type, deposition time or films thickness. All films show a high optical transmittance of 80-90% in the visible spectrum making them attractive for solar cell applications. Taking into account the different surface structure of glass or solar material, the presented growth mechanisms are still of importance for the understanding of the $In(OH)_xS_y$ buffer layer deposition in solar cells. Further work is in a progress to transfer the $In(OH)_xS_y$ deposition to $CuInS_2$ solar cells.

Acknowledgements

One of the authors T. Dedova would like to thank J. Wienke for the possibility to undertake this study at ECN research group. Financial support by the SUNRISE project, EC project NNE5-2002-00017, grant No. 5612 and MMTDK is gratefully acknowledged. The authors wish to thank M. Roos and O. Volobujeva for the SEM micrographs and H. Muffler and A. Mere for the fruitful discussions.

References

[1] N. A. Allsop, A. Schönmann, H.-J. Muffler, M. Bär, M.C. Lux-Steiner and Ch.-H. Fischer, Prog. Photovolt: Res. Appl. 13 (2005) 607-616.

[2] C. H. Huang, Sheng S. Li, W. N. Shafarman, C.-H. Chang, E. S. Lambers, L. Rieth, J. W. Johnson, S. Kim, B. J. Stanbery, T. J. Anderson, P. H. Holloway, Solar Energy Materials & Solar Cells 69 (2001) 131-137.

[3] D. Hariskos, M. Ruckh, U. Ruhle, T. Walter, H.W. Schock, J. Hedstrom, L. Stolt, Sol. Energy Mater. Sol. Cells 41/42 (1996) 345.

[4] M. Weber, J. Krauser, A. Weidinger, J. Bruns, C.H. Fischer, W. Bohme,J. Rohrich, R. Scheer, Journal of the Electrochemical Society 146, 6 (1999) 2131.

[5] Ramanathan, K., Hasoon, F.S., Smith, S., Young, D.L.,Contreras, M.A., Johnson, P.K., Pudov, A.O., Sites, J.R., J. Phys. Chem. Solids 64 (2003b) 1495–1498.

[6] K.Ramanathan, R. Bhattacharya, J.Granata, J. Webb, D. Niles,M.A. Contreras, H. Wiesner, F.Hasoon, R.Noufi, 26th IEEE PVSC, Anaheim, CA (1997) Proceedings 319–322.

[7] M. Bär, S. Lehmann, M. Rusu, A. Grimm, I.M. Kötschau, I. Lauermann, P. Pistor, S. Sokoll, L. Weinhardt, C. Heske, Ch. Jung, Ch.-H. Fischer, Th. Schedel-Niedrig, M. Ch. Lux-Steiner, Applied Physics Letters 86 (2005) 222107.

[8] B. Canava, J.-F. Guillemoles, E.-B. Yousfi, P. Cowache, H. Kerber, A. Loeffl, H.-W. Schock, M. Powalla, D. Hariskos, D. Lincot, Thin Solid Films 361-362 (2000) 187-192.

[9] S. Nishiwaki, A. Ennaoui, S. Schuler, S. Siebentritt and M. Ch. Lux-Steiner, Thin Solid Films 431-432 (2003) 296-300.

[10] T. Wada, Y. Hashimoto, S. Nishiwaki, T. Satoh, S. Hayashi, T. Negami and H. Miyake, Solar Energy Materials and Solar Cells 67 1-4 (2001) 305-310.

[11] C. Kaufmann, S. Neve, W. Bohne, J. Klaer, R. Klenk, C. Pettenkofer, J. Röhrich, R. Scheer, U. Störkel, P.J. Dobson, 28th IEEE Photovoltaic Solar Energy Conference, Anchorage (2000) Proceedings 688-691.

[12] R. Bayón, C. Maffiotte and J. Herrero**,** Thin Solid Films 403-404, 1 (2000) 339-343.

[13] N. J. Harrick, Appl. Opt.10 (10) (1971) 2344.

[14] Koichi Yamaguchi, Tsukasa Yoshida and Hideki Minoura, Thin Solid Films 431-432 (2003) 354-358.

[15] B. Asenjo, A.M. Chaparro, M.T. Gutierrez, J. Herero, C. Maffiotte, Electrochimica Acta 49 (2004) 737-744.

[16] L. Larina, K. H. Kim, K. H. Yoon, M. Konagai and B. T. Ahn, 3rd World Conference on Photovoltaic Energy Convention, Osaka, Japan, May 11-18 (2003).

[17] R. Bayón, C. Maffiotte and J. Herrero, Thin Solid Films 353 1-2 (1999) 100-107.

[18] P. O'Brien, J. McAleese, Journal of Materials Chemistry 8 (1998) 2309 – 2314.

[19] D. Lincot, R. O. Borges, J. Vedel, M. Ruckh, J. Kessler, K. O. Velthaus, D. Hariskos, H. W. Schock, 11-th European Photovoltaic Solar Energy Conf., Montreux (1992).

[20] G. A. Kitaev, A. A. Uritskaya, S. G. Mokrushin, Russ. J. Phys. Chem. 39 (1965) 1101.

[21] M. Froment, D. Lincot, Electrochim. Acta, 1995, 40, 1293.

[22] R. Bayón, C. Guillén, M. A. Martínez, A. Martínez-Chaparro, M. T. Gutiérrez and J. Herrero, Proceeding 1st World Conference and Exhibition on Photovoltaic Solar Energy conversion, Vienna 1998.

[23] C. H. Huang, Sheng S. Li, L. Rieth, A. Halani, M.L. Fisher, Jiyon Song, T.J. Anderson, and P.H. Hoplloway, *Conf. Record of the 28th* IEEE Photovoltaic Specialists Conference (2000) 696-699.

[24] C. D. Lokhande, A. Ennaoui, P. S. Patil, M. Giersig, K. Diesner, M. Muller and H. Tributsch, Thin Solid Films 340 1-2 (1999) 18-23.

[25] J. Sterner, J. Malmström, L. Stolt, Progress in Photovoltaics: Research and Applications 13 3 (2005) 179 –193.

[26] D. Bhattacharyya, S. Chaudhuri, A. K. Pal, Vacuum 43 (4) (1992) 313.

[27] S. Avivi, Y. Mastai, A. Gedanken, Chem. Mater. 12 (2000) 1229.

[28] R. Bayón and J. Herrero, Proceedings of the 11th Workshop on Quantum Solar Energy Conversion - (QUANTSOL'98) March 14-19 (1999) Wildhaus, Switzerland

[29] J. George, K. S. Joseph, B. Pradeep, T. Y. Palson, Phys. Stat. Sol. (a), 106 (1988) 123K.

Figure Captions

Fig. 1 SEM micrographs of $In(OH)_xS_y$ layers obtained from bath: a) A for 10 minutes, b) B for 15 minutes and c) C for 5 minutes

Fig. 2 SEM micrographs of $In(OH)_xS_y$ layers deposited for 30 minutes in bath : a) A, b) B and c) C

Fig. 3 Specular reflectance and fitting data of the $In(OH)_xS_y$ layers obtained by route A as an example for thickness determination

Fig. 4 Film thickness versus deposition time for A)'hot' start, B) 'cold' start and C) In-pretreatment prior the 'hot' start procedures

Fig. 5 Graphical determination of optical bandgap of $In(OH)_xS_y$ films obtained from bath A having the different thicknesses

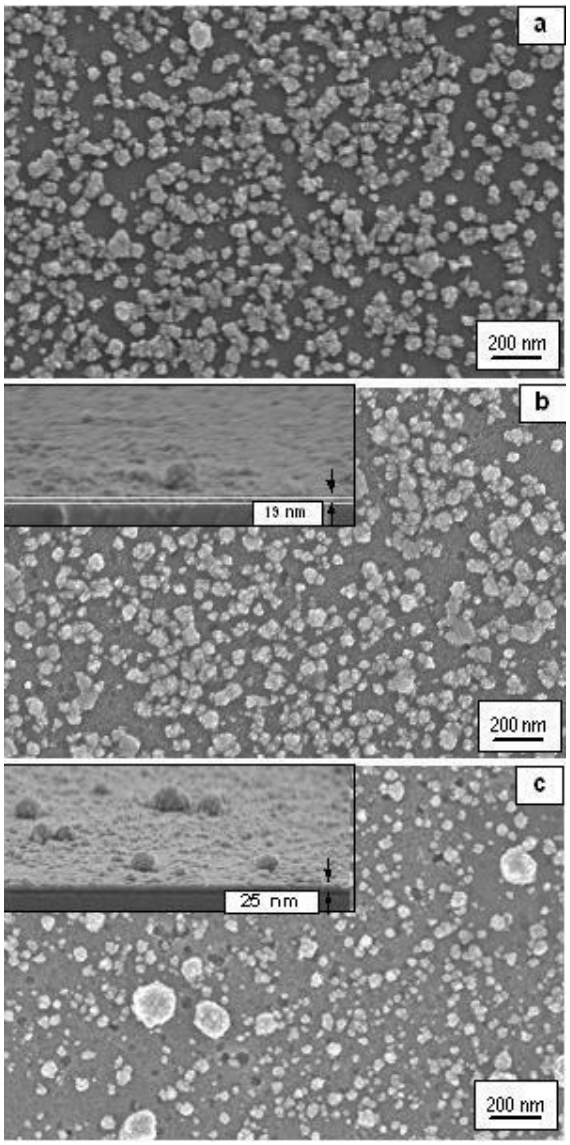

Fig. 1

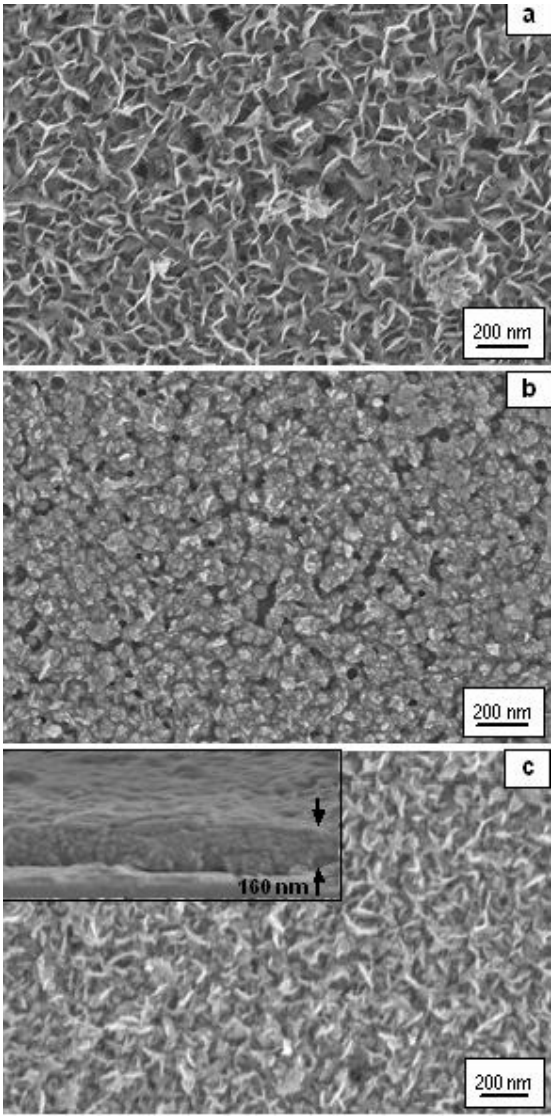

Fig. 2

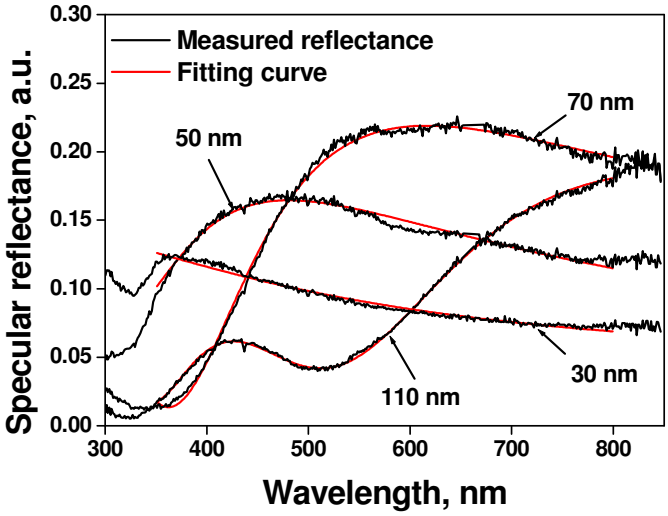
Measured reflectance
Fitting curve
70 nm
50 nm
30 nm
110 nm
Specular reflectance, a.u.
Wavelength, nm
0.00
0.05
0.10
0.15
0.20
0.25
0.30
300
400
500
600
700
800

Fig. 3

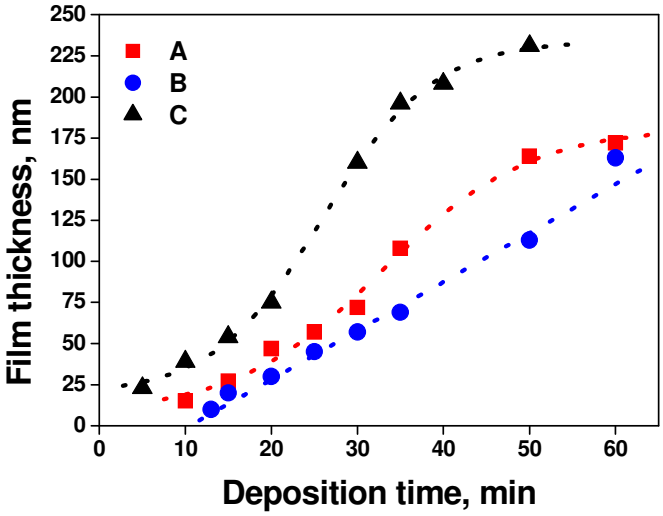
Film thickness, nm
Deposition time, min
A
B
C
0
25
50
75
100
125
150
175
200
225
250
0
10
20
30
40
50
60

Fig. 4

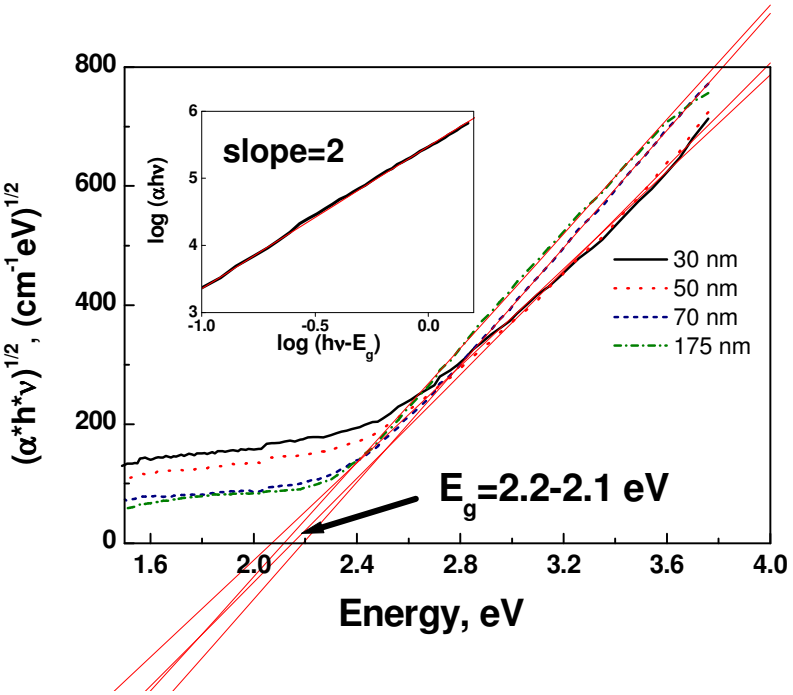
800
600
400
200
0
1.6
2.0
2.4
2.8
3.2
3.6
4.0
Energy, eV
(α*h*ν)^1/2 , (cm^-1eV)^1/2
E_g=2.2-2.1 eV
30 nm
50 nm
70 nm
175 nm
slope=2
log (α/hν)
log (hν-E_g)
6
5
4
3
-1.0
-0.5
0.0

Fig. 5